INTERNATIONAL JOURNAL FOR NUMERICAL METHODS IN FLUIDS
Int. J. Numer. Meth. Fluids 2005; **48**:61–83
Published online 14 February 2005 in Wiley InterScience (www.interscience.wiley.com). DOI: 10.1002/fld.935

A hybrid spectral/finite-difference to transient free-surface flow inside thin symmetric cavities of longitudinally varying thickness

Jie Zhang and Roger E. Khayat*,†

Department of Mechanical and Materials Engineering, The University of Western Ontario, London, Ont., Canada N6A 5B9

SUMMARY

The lubrication theory is extended for transient free-surface flow of a viscous fluid inside three-dimensional symmetric thin cavities of thickness that varies in the flow direction. The problem is first formulated for a cavity of arbitrary shape. The moving domain is mapped onto a rectangular domain at each time step of the computation. The pressure, which in this case is governed by the modified Laplace's equation, is expanded in a Fourier series in the spanwise direction. The expansion coefficients are obtained using the finite-difference method. Only a few modes are usually needed to secure convergence. The flow behaviour is strongly influenced by the cavity thickness. The flows inside a straight, contracting, expanding, and modulated cavities are examined. It is found that while the evolution of the front is always monotonic with time, that of the velocity at the front can be oscillatory if the degree of contraction of the cavity (whether modulated or not) is significant. The velocity of the contact point along the lateral walls is usually larger than that at the front, leading to the straightening of the front. However, for modulated cavities, the front may advance at a faster rate, leading to its own undulation.

KEY WORDS: spectral; finite difference; transient free surface flow; three dimensional; thin cavity flow; lubrication

1. INTRODUCTION

The modelling and simulation of free-surface cavity flow have been the object of considerable interest over the last two decades. The interest in this area of research activity is largely due to the need for our understanding of the flow during the fabrication of plastic parts as encountered in the processing industry, particularly in injection moulding. Modelling of the flow in these processes represent several major challenges since it is inherently transient,

*Correspondence to: Roger E. Khayat, Department of Mechanical and Materials Engineering, The University of Western Ontario, London, Ont., Canada N6A 5B9.
†E-mail: rkhayat@eng.uwo.ca

Received 16 July 2003
Revised 6 July 2004
Accepted 27 August 2004

non-isothermal, and includes a free surface moving through cavities of highly irregular geometry. Despite the continuous development of new solution techniques, and the advent of powerful computational platforms, the simulation of free-surface flow inside a cavity remains challenging. For transient free-surface flow, the presence of geometrical non-linearities, coupled to material non-linearities, such as inertia (die casting) and non-Newtonian (injection moulding) effects, make the moving-domain problem difficult to solve and understand.

Due to limited computational resources, the three-dimensional flow problem has customarily been simplified to a two-dimensional problem, based on the observation of Hele-Shaw [1–3]. The method is closely related to the lubrication or shallow-water theory for Newtonian flow [4]. In this approach, the cavity is assumed to be thin, and out of plane flows are neglected. Richardson [5] was the first to propose this method for moulding flow. He examined Newtonian, isothermal flow inside cavities of simple geometry. Three decades later, the lubrication assumption remains the basis for the simulation of free-surface flow of thin films [6–8]. Various flow configurations were analysed: Kamal and Kenig [9], Winter [10], and Berger and Gogos [11] have examined the case of radial flow from a central injection point. White [12], Broyer *et al.* [13], and Van Wijngaarden *et al.* [14], among others, have analysed the flow between parallel and non-parallel plates. Williams and Lord [15] studied the flow in circular channels.

There have been several notable studies of the flow inside cavities of complex shape. In one study, the mould geometry is laid flat and then described through a series of simpler geometries: radial flow, flow between parallel plates and flow in circular channels [16, 17]. The finite-element has been used to simulate the Hele-Shaw flow as applied to injection and compression mould filling [18, 19]. Given the moving boundaries involved, it is necessary to generate a new mesh after each successive time step. The cost and inconvenience of finite-element remeshing has led to the use of the boundary-element techniques in general cavity flow [20, 21], and the Hele-Shaw flow in particular [22, 23]. While the BEM has obvious advantages over conventional domain methods for the treatment of moving-boundary problems, it suffers from severe drawbacks, the most notable of which is its lack of capability to handle non-linearities such as inertia and non-Newtonian effects, or even a cavity of variable thickness. Hence, the simulation of transient free-surface flows remains challenging since, on the one hand, conventional domain methods are inadequate for adaptive meshing, and, on the other hand, integral methods such as the BEM, which can handle more easily adaptive meshing, cannot incorporate non-linearities from the governing equations. As a result, the physical flow remains poorly understood.

In the present paper, the difficulties with conventional methods are addressed for the flow inside thin cavities of arbitrary thickness. A hybrid Lagrangian/Eulerian method is proposed, which consists of mapping the irregular moving domain, at each time step, onto a fixed rectangular domain. The flow is expanded in Fourier series in the spanwise direction, and the finite-difference method is used to obtain the expansion coefficients. The method is used to obtain the three-dimensional flow field inside a thin cavity of variable thickness. This corresponds to the solution of a large class of free-surface flow problems, with close relevance to polymer processing. The flow is typically encountered during the filling stage inside a thin cavity as in injection moulding. The lubrication assumption is adopted to derive the resultant equations for a Newtonian fluid, averaged over the thickness of the cavity. The influence of cavity thickness is particularly explored. The flow field is examined for the case of flat, contracting, expanding, and modulated cavities.

2. PROBLEM FORMULATION

In this section, the basic assumptions for the lubrication are first briefly reviewed for viscous fluids. The theory is then extended to include the transient free-surface flow inside thin three-dimensional cavities of arbitrary shape. The case of symmetric cavities with thickness varying streamwise will then be considered in detail.

2.1. General lubrication formulation

Consider an incompressible Newtonian fluid of viscosity μ. Inertia effects are assumed negligible. The lubrication assumption, which is the hydrodynamic analog of thin-shell theory, is applied to determine the flow. In most lubrication films the thickness of the film is small compared with its lateral dimensions. Properly handled, this observation can be used to eliminate from the hydrodynamic equations and boundary conditions the dependence upon one of the three spatial variables. The continuity equation is integrated across the film and the Navier–Stokes equation is used to evaluate the quantities appearing as integrands. The conservation equations are formulated in the narrow-gap limit. These equations are first cast in terms of dimensionless variables. Typically, in thin-cavity flow, there are three characteristic lengths, L_1 and L_2 along the lateral directions, and H, representing the thickness of the cavity in the third (depthwise) direction. It is usually assumed that L_1 and L_2 are of the same order, L, say. In this case, L and H will be taken as the reference length and thickness in the horizontal and vertical directions, respectively, with (x, y) and z being the corresponding dimensionless co-ordinates. The horizontal, (u_x, u_y), and vertical, u_z, velocity components are scaled by V and εV, respectively, where V is a reference velocity, and $\varepsilon = H/L$ is the typical aspect ratio in the problem. The time, t, is scaled by L/V, and the pressure, p, is scaled by $\mu V/L\varepsilon^2$. The position vector of a general point in space is denoted by $\mathbf{r}(x, y, z)$, and its projection in the (x, y) plane is denoted by $\mathbf{x}(x, y)$.

Figure 1 illustrates schematically the general flow and notations used. The figure shows a step of the filling stage of a thin cavity of general shape. At any time, the fluid fills the domain that is delimited the exit, Γ_e, cavity wall Γ_w, and front Γ_f. If terms of $O(\varepsilon^2)$ and higher are excluded, and in the absence of inertia, the conservation equations reduce to the following equation for the pressure [4]:

$$(h^3 p_{,x})_{,x} + (h^3 p_{,y})_{,y} = 0 \tag{1}$$

where $h = h(\mathbf{x})$ is the prescribed dimensionless thickness of the cavity. Note that the pressure $p(\mathbf{x}, t)$ is reduced to its hydrostatic part and does not vary with the vertical direction, z. The velocity components are given by

$$u_\alpha(x, y, z, t) = \frac{p_{,\alpha}(x, y, t)}{2}\,[z - h_1(x, y)][z - h_2(x, y)], \quad \alpha = x, y \tag{2}$$

where $h_1(\mathbf{x})$ and $h_2(\mathbf{x})$ are the heights of the lower and upper cavity surfaces, respectively (see Figure 1). Note that $h(\mathbf{x}) = h_2(\mathbf{x}) - h_1(\mathbf{x})$. If the thickness is constant, then the pressure becomes governed by Laplace's equation. The problem thus reduces to the determination of

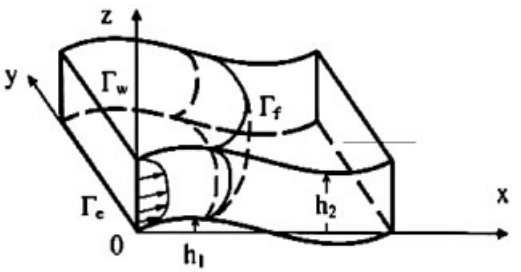

Figure 1. Schematic illustrating the transient free-surface flow inside a cavity induced by the imposed flow at the cavity entrance, Γ_e.

the scalar variable, $p(\mathbf{x},t)$. This is a quasi-steady problem since the time dependence is not explicit in the pressure equation.

2.2. Domain of computation

For simplicity, the cavity is assumed to have straight lateral edges and symmetric with respect to the (x,y) plane. The cavity thickness is also assumed to vary with x. Thus, $h_2(\mathbf{x}) = -h_1(\mathbf{x}) = h(x)/2$. The domain of computation is obviously the projection, $\Omega_{xy}(t)$, of the physical domain $\Omega(t)$ onto the (x,y) plane. The front shape at any time is generally given by $x = X(y,z,t)$. In the (x,y) plane, this the shape of the front is given by $x = L(y,t) \equiv X(y,z=0,t)$ be the shape of the front. The domain of computation becomes $\Omega_{xy}(t) = \{(x,y) \mid x \in [0,L],\ \ y \in [0,2\pi]\}$.

2.3. Boundary and initial conditions

The lubrication formulation does not accommodate adherence conditions at the lateral walls. Stick boundary conditions can only be applied at the bottom and upper rigid cavity surfaces. In this case, only the no-penetration condition applies along the lateral walls. This assumption is not as unrealistic as it seems at first, since flow core in a thin cavity is not significantly affected by the boundary-layer region at the lateral walls. The flow is assumed to be driven by an imposed (dimensionless) pressure gradient, $q_0(y,z,t)$, at $x = 0$, so that the general boundary condition at the entrance to the cavity is given by

$$q(x=0,y,z,t) = q_0(y,z,t), \quad \mathbf{x} \in \Gamma_e \tag{3}$$

where $q = \mathbf{n} \cdot \nabla p$ is the normal directional derivative of the pressure, with $\mathbf{n}$ being the normal vector to Γ_e. The pressure gradient may be either maintained fixed at all time, or adjusted according to the flow conditions inside the cavity (mould). A time-dependent pressure gradient corresponds typically to the inlet condition in injection moulding where the pressure rather than the flow rate is varied with time at the source of fluid. Although a variable pressure gradient can be easily accommodated by the present formulation, q_0 will be assumed to depend only on y. Thus, at the entrance to the cavity, $q_0(y,t) = -p_{,x}(x=0,y,t)$. In this work, condition (3) is assumed to be of the form

The pressure gradient rather than the flow rate is imposed by prescribing $p_{,x}$ at $x=0$. In this work, the following expression is adopted:

$$p_{,x}(x=0,y,t)=-q_0(y,t)=y(y-2\pi) \tag{4}$$

Since the lubrication assumption can only accommodate the no-penetration conditions at the lateral walls, then

$$q(\mathbf{x},t)=\mathbf{n}(\mathbf{x},t)\cdot\nabla p(\mathbf{x},t)=0, \quad \mathbf{x}\in\Gamma_{\mathrm{w}}(t) \tag{5}$$

where $\mathbf{n}$ is the unit normal to $\Gamma_{\mathrm{w}}(t)$. At the lateral walls, Equation (5) yields in this case

$$p_{,y}(x,y=0,t)=p_{,y}(x,y=2\pi,t)=0 \tag{6}$$

At the front (free-surface) the imposition of a suitable dynamic condition is not obvious for thin-cavity flow. It is clear that for the general three-dimensional flow, and in the absence of surface tension effect, a zero-traction condition must apply at the front. Let $\mathbf{n}(\mathbf{r},t)$ be the unit normal vectors to the front, $\Gamma_{\mathrm{f}}(t)$. In absence of surface tension effect, the traction, $\mathbf{t}$, must vanish at the front, or

$$\mathbf{t}(\mathbf{r},t)=0, \quad \mathbf{r}\in\Gamma_{\mathrm{f}}(t) \tag{7}$$

To leading order, however, the dynamic condition reduces to the vanishing of the pressure at the free-surface [4]. This condition is conveniently taken as

$$p(x=L,y,t)=0 \tag{8}$$

There remains the kinematic condition at the free-surface, which is the least obvious among the boundary conditions to implement. In a Lagrangian representation, such as the present formulation, the moving boundary is assumed to deform with the fluid velocity, such that the evolution of $\Gamma_{\mathrm{f}}(t)$ is governed by the equation

$$\frac{\mathrm{d}\mathbf{r}}{\mathrm{d}t}=\mathbf{u}(\mathbf{r},t), \quad \mathbf{r}\in\Gamma_{\mathrm{f}}(t) \tag{9}$$

where $\mathbf{u}$ is the velocity vector. The following form of the kinematic condition (9) will then be used in this work:

$$U_x(y,z,t)=X_{,t}(y,z,t)+U_y(y,z,t)X_{,y}(y,z,t) \tag{10}$$

where $U_\alpha(y,z,t)=u_\alpha(x=X,y,z,t)$ are the velocity components at the front. It is important to observe that the z dependence in Equation (10) is implicit, and that X is regarded as dependent on x and y for a given z value. Equation (10) gives explicitly the three-dimensional shape of the front. However, only $L(y,t)$ is needed in order to solve for the pressure. The relevant kinematic condition then reduces to

$$L_{,t}(y,t)+V(y,t)L_{,y}(y,t)=U(y,t) \tag{11}$$

where the velocity components at the front in the (x,y) plane are introduced as

$$U(y,t)=U_x(y,z=0,t) \quad \text{and} \quad V(y,t)=U_y(y,z=0,t) \tag{12}$$

Although easy to implement, the resulting scheme based on Equation (9) tends to sweep points on the moving boundary along the tangent to the moving boundary, even if only small

shape changes take place. Consequently, frequent redistribution of the moving-boundary points or remeshing would be necessary when relation (9) is used. In the current study, the difficulty of node sweeping will be easily circumvented as will be observed below.

Regarding the initial conditions for the problem, it is clear from Equations (1), (2) and (11), that the initial shape of the front is the only condition needed. Ideally, the computation should begin with the front coinciding with the entrance to the cavity, ready to flow under the action of a prescribed pressure or velocity distribution. However, this would correspond to a zero initial domain, $\Omega(t=0)=0$, and no initial discretization can be performed (for instance, if a finite-difference or element scheme is envisaged). In this work, the fluid is assumed to occupy a small portion of the cavity. The initial amount and front shape of the fluid are not crucial over the long time. Similarly to injection moulding, the pressure rather than the flow rate will be prescribed at the (die) exit, as in Equation (4), and will be assumed maintained at all time. The initial domain occupied by the fluid in the (x, y) plane is taken to correspond to $\Omega_{xy}(t=0)=\{(x,y)|x\in[0,L(y,t=0)],\ y\in[0,2\pi]\}$, where $L(y,t=0)$ is the initial shape of the front, which will be prescribed later.

3. SOLUTION PROCEDURE

The lubrication problem is solved by first mapping the flow domain onto a rectangular domain. A modified pressure is introduced, which reduces to the pressure when the cavity thickness is constant. The method of Galerkin projection is used, whereby the modified pressure is expanded in Fourier series. The expansion coefficients are then determined by solving the projected pressure equation. Once $p(\mathbf{x},t)$ is determined from Equation (1), at a given time, t, the velocity components are then determined. Particularly, the velocity components at the front are required in order to determine the evolution of the front.

3.1. Domain mapping

In order to represent the modified pressure, S, in series of orthonormal functions, the domain of computation must be rectangular. For this, the physical domain $(x, y)\in\Omega_{xy}(t)$ is mapped onto the domain $(\xi,\zeta)\in[0,1]\times[0,2\pi]$. The mapping is schematically shown in Figure 2. Thus,

$$\xi(x,y)=\frac{x}{L(y,t)},\quad \zeta(x,y)=y \tag{13}$$

Upon use of expressions (13), Equation (1) for the modified pressure reads

$$[1+(\xi L_{,\zeta})^2]p_{,\xi\xi}+\left[2\xi(L_{,\zeta})^2-\xi LL_{,\zeta\zeta}+3\frac{h_{,\xi}}{h}\right]p_{,\xi}-2\xi LL_{,\zeta}p_{,\xi\zeta}+L^2p_{,\zeta\zeta}=0 \tag{14}$$

subject to the following boundary conditions:

$$p_{,\xi}(\xi=0,\zeta,t)=\zeta(\zeta-2\pi) \tag{15}$$

$$p(\xi=1,\zeta,t)=p_{,\zeta}(\xi,\zeta=0,t)=p_{,\zeta}(\xi,\zeta=2\pi,t)=0 \tag{16}$$

Note that p is coupled to the shape of the front, $L(y,t)$, which must be determined as part of the solution, thus making the problem nonlinear. The shape of the front in turn delimits the

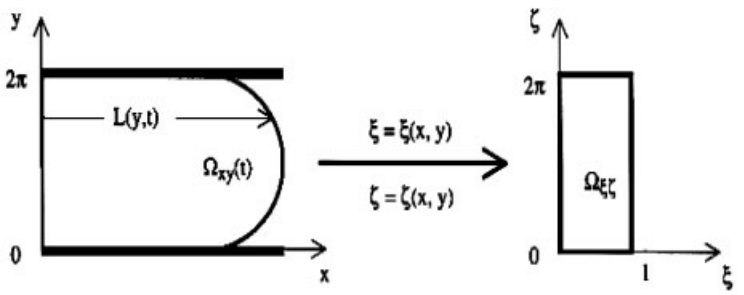

Figure 2. Mapping of the middle slice of the time-dependent physical domain in the (x, y) plane onto the rectangular computational domain in the (ξ, η) plane.

domain in the (x, y) plane. Once $p(x, y, t)$ is obtained at a given time, the horizontal velocity components at the front are evaluated. $L(y, t)$ is then determined by solving the kinematic condition.

3.2. Pressure expansion

The modified pressure can be expressed as

$$p(\xi, \zeta, t) = \sum_{n=0}^{\infty} p_n(\xi, t) \cos(n\zeta) \tag{17}$$

Note that expression (17) satisfies the two lateral boundary conditions (16). Obviously, a truncation level will have to be imposed, leading to a finite number of modes, N, in the expansion. If expression (17) is substituted into Equation (14), and the Galerkin projection method is used, then the following recursive relation is obtained for the pressure coefficients:

$$\sum_{n=0}^{N} A_{mn} p_{n,\xi\xi} + \sum_{n=0}^{N} B_{mn} p_{n,\xi} + \sum_{n=0}^{N} C_{mn} p_n = 0 \tag{18}$$

where $m \in [1, N]$, and the time-dependent coefficient matrices are given by

$$\begin{aligned} A_{mn}(\xi, t) &= \langle \cos(m\zeta) \cos(n\zeta)[1 + (\xi L_{,\zeta})^2] \rangle \\ B_{mn}(\xi, t) &= \left\langle \cos(m\zeta) \left\{ \left[2\xi (L_{,\zeta})^2 - \xi L L_{,\zeta\zeta} + 3 \frac{h_{,\xi}}{h} \right] \cos(n\zeta) + 2nLL_{,\zeta} \sin(n\zeta) \right\} \right\rangle \\ C_{mn}(t) &= -n^2 \langle L^2 \cos(n\zeta) \cos(m\zeta) \rangle \end{aligned} \tag{19}$$

where the notation $\langle\ \rangle = \int_0^{2\pi} \mathrm{d}\zeta$ is used. In this case, the Galerkin projection consists of multiplying Equation (14) by $\cos(m\zeta)$ for $m \in [1, N]$, and integrating it with respect to ζ from 0 to 2π, after substituting expression (17). The boundary conditions for system (18) are deduced from conditions (15) and (16), leading to

$$p_n(\xi = 1, t) = 0 \tag{20}$$

$$p_{n,\xi}(\xi = 0, t) = \langle \zeta(\zeta - 2\pi) \cos(n\zeta) \rangle \tag{21}$$

Once Equation (18) is solved, $p(\mathbf{x},t)$ is determined over the domain $\Omega_{xy}(t)$, in particular along the front $x=L(y,t)$, which in turn allows the determination of the velocity at the front. Similarly to the pressure expansion (17), $L(\zeta,t)$, is expanded as:

$$L(\zeta,t)=\sum_{n=0}^{N} L_n(t)\cos(n\zeta) \tag{22}$$

The Galerkin projection is used to solve Equation (17), and the coefficients $L_n(t)$ are governed by following set of coupled ODEs:

$$\frac{\mathrm{d}L_m(t)}{\mathrm{d}t}=\sum_{n=0}^{N} D_{mn}(t)L_n(t)+E_m(t), \quad m\in[1,N] \tag{23}$$

where the coefficients are given by

$$\begin{aligned} D_{mn}(t)&=n\langle\cos(m\zeta)\sin(n\zeta)V(\zeta,t)\rangle \\ E_m(t)&=\langle\cos(m\zeta)U(\zeta,t)\rangle \end{aligned} \tag{24}$$

The initial condition needed are based on the shape of the front, which in this work is assumed to be

$$L(y,t=0)=1+\left(\frac{y}{\pi}\right)^4-4\left(\frac{y}{\pi}\right)^3+4\left(\frac{y}{\pi}\right)^4 \tag{25}$$

There are thus N initial conditions needed for the problem, which take the form

$$L_n(t=0)=\langle\cos(n\zeta)L(\zeta,t=0)\rangle/\pi \tag{26}$$

The problem clearly reduces to a set of coupled equations (18) and (23) involving $2N$ unknowns, which may be solved implicitly or explicitly with time. It is found that an implicit scheme is not necessary for the present problem. A forward explicit finite-difference in time is used to solve Equation (23). In this case, system (18) constitutes a set of N partial differential equations in ξ and t. However, since time is not explicitly apparent, the system can be regarded as a set of $2N$ first-order ordinary differential equations in ξ at a given time, t. This is a two-point boundary-value problem, which is solved using a variable order, variable step size finite-difference method in ξ, with deferred corrections (IMSL-DBVPFD). The numerical assessment of the method is covered in the next section.

4. NUMERICAL ASSESSMENT AND RESULTS

The transient free-surface flows inside thin cavities of constant and variable thickness are examined. The influence of cavity thickness is investigated for the flow inside a cavity of constant thickness, the flow inside expanding and contracting cavities, and the flow inside a modulated cavity. All results are given in terms of dimensionless quantities. Although the flow behaviour inside a flat cavity is somewhat predictable, it will be studied in some detail since it constitutes a reference base for the more complicated flow inside cavities with variable thickness. In addition, the results allow a close quantitative assessment of the flow in simple cavities.

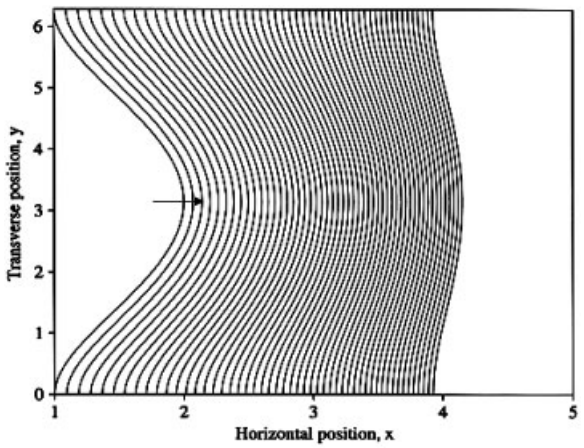

Figure 3. Transient flow inside a flat plate with initial curved domain. The fronts are shown at equal time intervals over a period of 5 time units. The arrow in this and subsequent figures indicates the time direction.

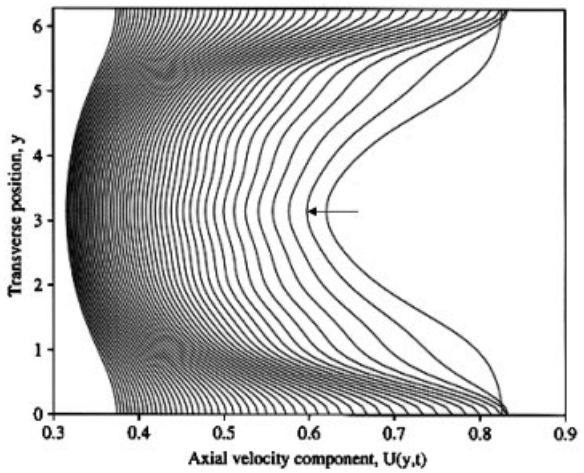

Figure 4. Distribution of the streamwise velocity component, $U(y,t)$, at the front for $0<t<5$, for the flow corresponding to Figure 3.

4.1. Flow inside a flat cavity

Consider the flow inside a cavity of constant thickness. The length and the width are taken to lie along the x and y directions, respectively (see Figure 2). The thickness of the cavity is assumed to be constant, so that $h_1 = 0$, and $h_2 = 1$. Although the fluid is flowing predominantly in the x direction, there is a strong secondary flow in the y direction as well. Figure 3 shows the evolution of the front in the (x, y) plane between the two flat plates at $z = 0.5$. The front

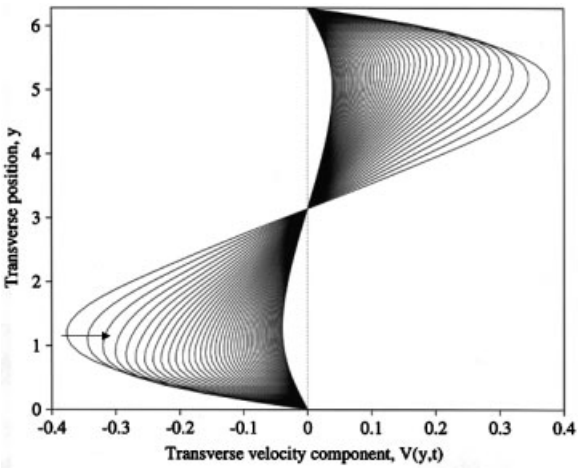

Figure 5. Distribution of the lateral spanwise velocity component, $V(y,t)$, at the front for $0<t<5$, for the flow corresponding to Figure 3.

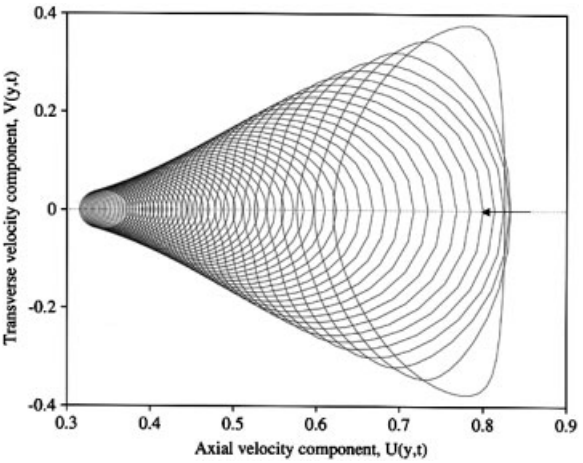

Figure 6. Phase plots of the streamwise and lateral velocity components, $U(y,t)$ and $V(y,t)$, at the front for $0<t<5$, for the flow corresponding to Figure 3.

is shown at equal intervals over a period of 5 time units. Note that the initial domain is shown only partially for clarity since it extends to $x=0$. The figure indicates a relatively dominant streamwise flow at the walls (slip) $y=0$ and 2π, leading to the straightening of the front with time despite the parabolic driving pressure gradient at the entrance $x=0$. The lateral flow tends to diminish in intensity with fluid advancement. The figure also indicates a decrease in front advancement rate with time.

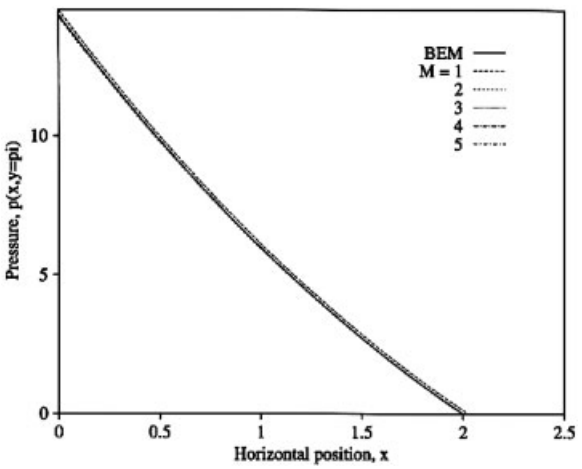

Figure 7. Pressure along the centre of the domain ($y = \pi$) for the stationary flow inside a flat plate based on five levels of truncation, $M = 1, 2, 3, 4$ and 5. The distribution based on the BEM is also included.

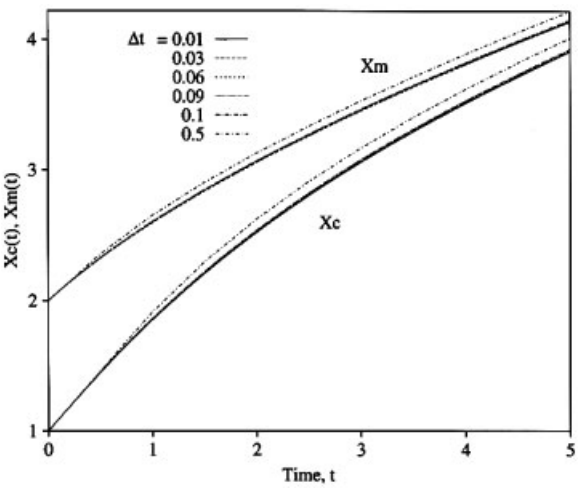

Figure 8. Evolution of the front tip position, X_m, and the contact position, X_c, with time for the flow inside a flat plate ($M = 5$). The figure shows the influence of the time increment for the range $\Delta t \in [0.01, 0.5]$.

The flow field at the front is further appreciated by examining the velocity components at the front. Figures 4 and 5 show the distributions of the streamwise and spanwise components at the front, $U(y,t)$ and $V(y,t)$, respectively. The difference between the velocity of the front tip, $U(\pi,t)$ and that of the points of contact, $U(0,t)$ and $U(2\pi,t)$, is obvious from Figure 4. The figure shows that $U(\pi,t)$ is roughly 30% smaller than $U(0,t)$ and $U(2\pi,t)$ in the initial

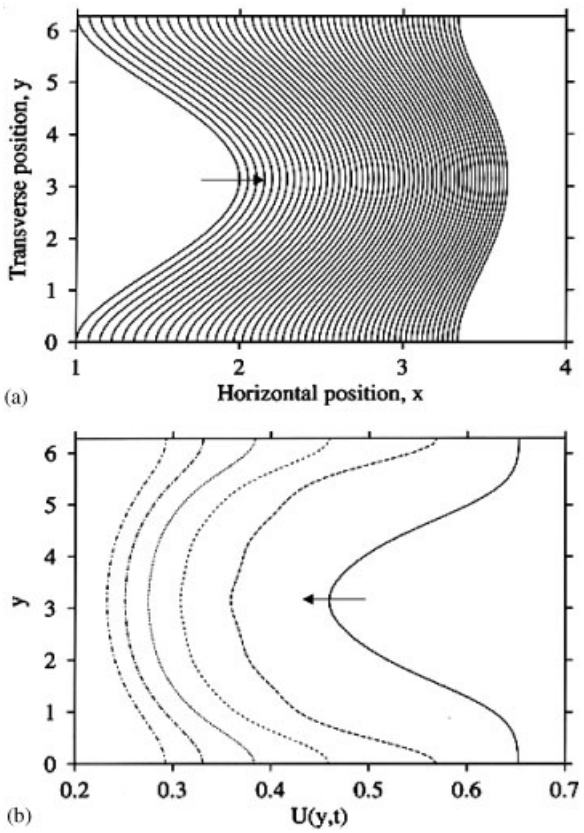

Figure 9. Flow inside an expanding cavity with slope = 0.1: (a) the fronts are shown at equal time intervals over a period of 5 time units; and (b) distribution of the streamwise velocity component, $U(y,t)$, at the front at $t = 0, 1, 2, 3, 4$ and 5 (see legends in Figure 10(a)).

stages. This difference decreases with time (with the straightening of the front). It is interesting to observe that the velocity of the contact point increases initially before decreasing with time. The maximum reached depends on the shape of the cavity as will be seen below. The figure also shows that the velocity tends to level off in the long time. The velocity component along the spanwise direction, $V(y,t)$, is strongest initially, and is generally of the same order of magnitude as $U(y,t)$, as depicted from Figure 5. As expected, the spanwise velocity vanishes at $y = 0$ and $y = 2\pi$. It decreases considerably in the later stages. The rate of decrease is strongest initially. The overall nonlinear behaviour is reflected in Figure 6, which shows the phase plot in the (U, V) plane. Each phase plot gives the behaviour of the velocity components along the front at a given time. The closed cycles decrease in overall diameter, and move closer to the V-axis, confirming the weakening of the flow with time. Initially, the cycles are distorted, indicating the presence of strong non-linearities. The cycles gradually adopt the shape of ellipses, reflecting the linear behaviour of a harmonic oscillator.

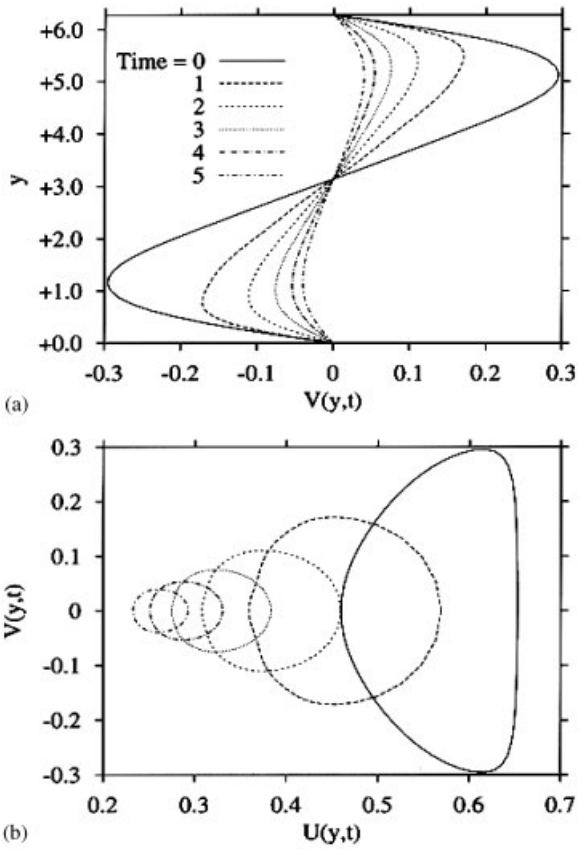

Figure 10. (a) Distribution of the spanwise velocity component, $V(y,t)$, at the front for the flow corresponding to Figure 9(a); and (b) phase plots of the streamwise and lateral velocity components, $U(y,t)$ and $V(y,t)$.

The accuracy of the results and convergence of the method are assessed by examining the influence of the number of modes and time increment in the finite-difference scheme. The comparison is also carried out against results based on the BEM for a fixed domain. Figure 7 shows the influence of the number of modes, M, on the pressure distribution, $p(x, y=\pi)$, along the horizontal direction x inside the initial domain (at $t=0$). There is a significant discrepancy between the solution based on $M=1$ and those based on $M>1$. When $M=1$, the pressure is overestimated. The error is uniform with respect to x. Moreover, the front tip position slightly exceeds $x=2$ as a result of the poor representation of the front shape. The inclusion of higher-order modes leads to good agreement with the BEM solution. Convergence is essentially attained for $M>2$. This fast rate of convergence is typical of thin-cavity flow, including the flow inside a cavity of variable thickness. However, additional modes are needed for more complex cavity shapes.

The influence of the time increment, Δt, is assessed in Figure 8, where the evolution of the horizontal position, X_c, of the contact point between the moving front and solid wall,

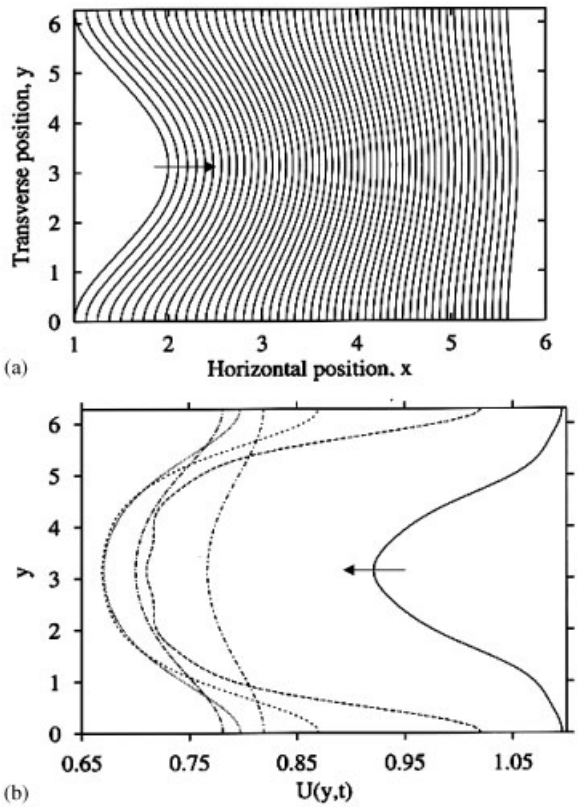

Figure 11. Flow inside a contracting cavity with slope $= -0.1$: (a) the fronts are shown at equal time intervals over a period of 5 time units; and (b) distribution of the streamwise velocity component, $U(y,t)$, at the front at $t = 0, 1, 2, 3, 4$ and 5 (see legends in Figure 12(a)).

and that of the front tip, X_m, are plotted against time for $\Delta t \in [0.01, 0.5]$ over a period of 5 time units. Convergence is attained for $\Delta t \leqslant 0.1$. The contact point between the front and lateral walls moves at a faster rate than the front tip initially as shown in Figure 8. The rate of advancement, $\mathrm{d}X_c/\mathrm{d}t$, tends, however, to decrease with time, and eventually becomes comparable to $\mathrm{d}X_m/\mathrm{d}t$, reflecting the straightening of the front (see Figure 3). Based on the above results and additional numerical assessment for other flow configurations, all the results reported in this work are obtained with $M = 5$ and $\Delta t = 0.1$.

4.2. Flow inside expanding and contracting cavities

So far, all results reported above have been restricted to a cavity of constant thickness, $h(\mathbf{x}) = 1$ and flat walls. In this section, the cavity thickness is varied with x linearly. The influence of a variable thickness can be intricate given the local character of the flow. Two types of thickness distributions will be investigated, corresponding to linearly diverging, and linearly converging walls. Consider then the flow inside a cavity of thickness $h(\mathbf{x}) = ax + 1$, where a is the slope of inclination of the cavity walls.

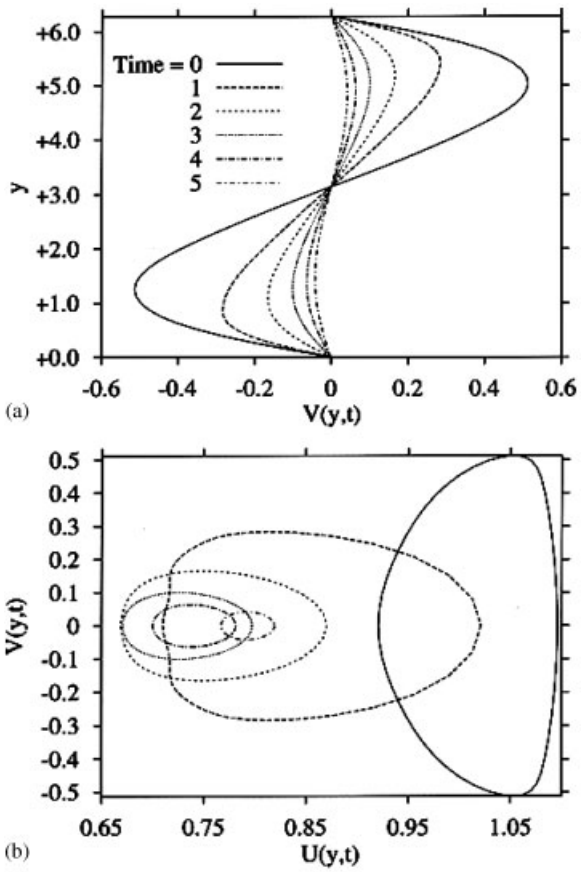

Figure 12. (a) Distribution of the spanwise velocity component, $V(y,t)$, at the front for the flow corresponding to Figure 11(a); and (b) phase plots of the streamwise and lateral velocity components, $U(y,t)$ and $V(y,t)$.

Consider first the flow inside an expanding cavity, with $a = 0.1$. The evolution of the front and the velocity field at the front are depicted in Figures 9 and 10. The results should be compared with those corresponding to a flow inside a flat plate (Figures 3–6). Qualitatively, the expansion does not seem to cause a significant change in flow behaviour. However, a deeper insight is gained regarding the correlation between front shape and velocity. First, the front position in Figure 9(a) indicates an overall decrease of (roughly) 10% in flow because of the expansion. However, the streamwise velocity distributions in Figure 9(b) hint to a decrease of 30%. On the one hand, in this case the discrepancy is larger between the velocity of the front tip and that of the contact point. Thus, the expansion causes a delay in the straightening of the front. On the other hand, the spanwise flow is weaker as a result of the expansion (compare Figures 10(a) and 5). This is not intuitively obvious since one expects the spanwise flow to be stronger at a front with higher curvature. The phase plots in

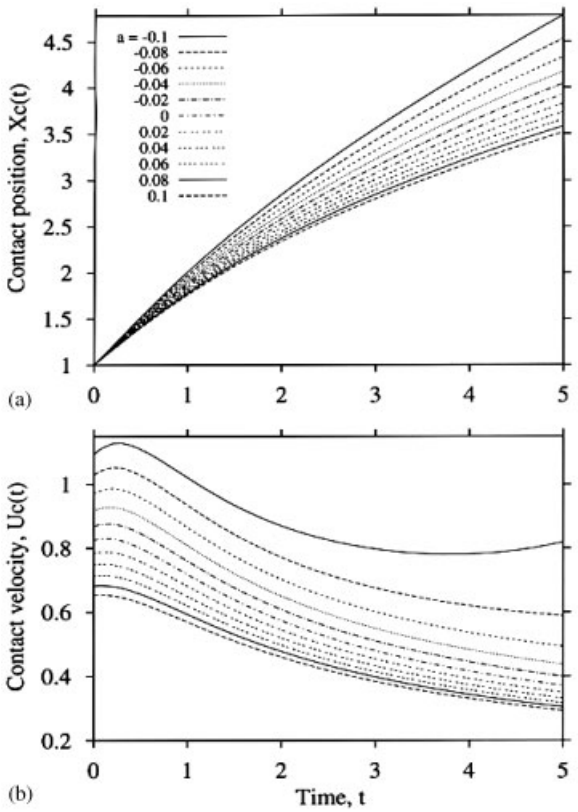

Figure 13. Influence of cavity slope for contracting, flat and expanding cavities for slope $a \in [-0.1, 0.1]$: (a) evolution of the contact point position, X_c, with time; and (b) velocity at the contact point position, $\mathrm{d}X_c/\mathrm{d}t$, with time.

Figures 10(b) and 6 also confirm these observations. This trend in flow behaviour becomes even more obvious once the case of contracting flow is examined.

The results corresponding to a flow inside a contracting cavity are shown in Figures 11 and 12 for $a = -0.1$. The flow is obviously much faster in this case (Figure 11(a)), approximately 30% faster than the flow inside a flat cavity. More interestingly, the streamwise velocity reaches a minimum and increases again with time (Figure 11(b)). This is in sharp contrast to the flow inside a flat and expanding cavities, where $U(y,t)$ decreases monotonically with time (see Figures 4 and 9(b)). The velocity of the contact point decreases dramatically relatively to that of the front tip after flow inception. The difference in velocity is not necessarily accompanied by an increase in spanwise flow (see Figure 12(a)). The difference, however, diminishes with time. The spanwise flow continues to gain in strength with cavity contraction, and, unlike U, V decreases monotonically with time (Figure 12(a)). The phase plots in Figure 12(b) reflect a significant level of non-linearity in contracting flow. The non-linearity also manifests itself in the form of undulations in the streamwise velocity distribution. The non-linearity is not limited to the initial stage as in Figures 6 and 10(b).

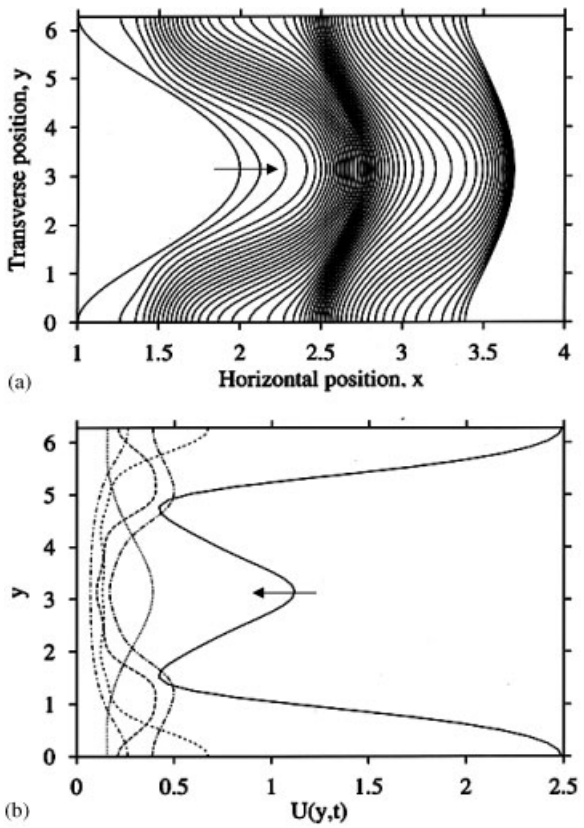

Figure 14. Flow inside a modulated cavity ($A = 0.2$ and $\omega = 6$): (a) the fronts are shown at equal time intervals over a period of 5 time units; and (b) distribution of the streamwise velocity component, $U(y,t)$, at the front at $t = 0, 1, 2, 3, 4$ and 5 (see legends in Figure 15(a)).

The overall influence of the wall slope, a, on the flow is illustrated in Figure 13. The figure displays the evolution of the contact point position, $X_c(t)$, (Figure 13(a)) and that of its velocity, $U_c(t)$ (Figure 13(b)) for the range $a \in [-0.1, 0.1]$, including the case of a flat cavity ($a = 0$). Figure 13(a) shows the overall decrease in X_c as a increases from -0.1. The decrease is sharpest near $a = -0.1$; a saturation is observed near $a = 0.1$. This means that, in practice, the flow intensifies quickly with cavity contraction. This intensification becomes more obvious by inspecting the overall velocity distributions in Figure 13(b). The velocity at the lateral walls exhibits generally a maximum initially, and then drops thereafter with time. This maximum strengthens with cavity contraction, and gradually disappears as a increases. There is also a weak minimum at the later stages, which becomes more pronounced with cavity contraction. The overall influence of a is stronger on U_c than on X_c. Similar conclusions can be drawn upon examination of the position and velocity of the front tip.

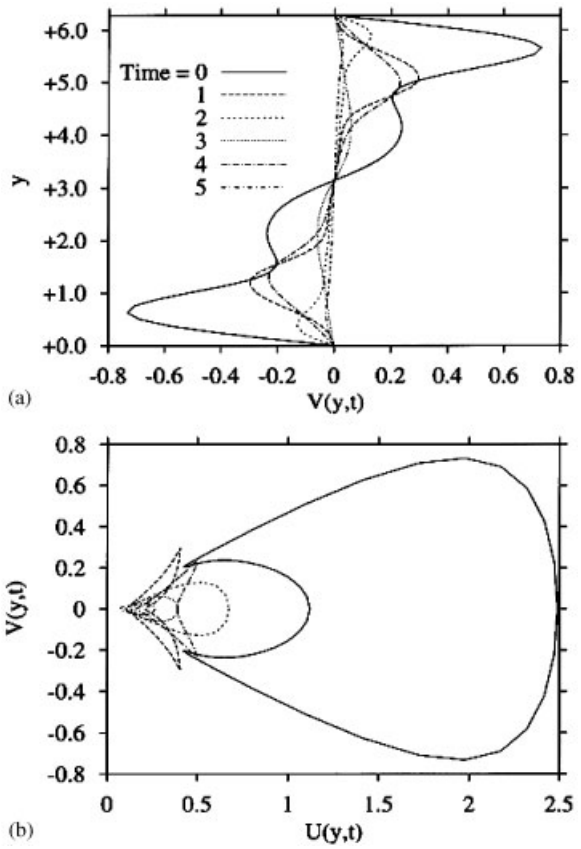

Figure 15. (a) Distribution of the spanwise velocity component, $V(y,t)$, at the front for the flow corresponding to Figure 14(a); and (b) phase plots of the streamwise and lateral velocity components, $U(y,t)$ and $V(y,t)$.

4.3. Flow inside an undulated cavity

For the flow inside a cavity with modulated walls, the thickness is taken as $h(\mathbf{x}) = 1 - A\sin(\omega x)$, where A is the amplitude and ω is the frequency of modulation. Figure 14(a) shows the evolution of the front for $A = 0.2$ and $\omega = 6$. The wall modulation gives rise to the additional waviness of the front. Overall, the successive front curves tend to disperse during a contraction of the cavity ($X_m < 2.4$ and $3 < X_m < 3.3$), and compress during an expansion of the cavity ($2.4 < X_m < 3$ and $X_m > 3.3$). More interestingly, the response of the movement along the walls is not in phase with that of the front tip. Indeed, the front curves near the wall tend to disperse (compress) later than near the tip.

The dynamic response becomes more obvious from Figures 14(b) and 15, which shows the evolution of the velocity components at the front (Figures 14(b) and 15(a)) and corresponding phase plots (Figure 15(b)). The results are again shown for $A = 0.2$ and $\omega = 6$. Upon flow inception ($t = 0$), the velocity experiences a significant jump because of cavity contraction.

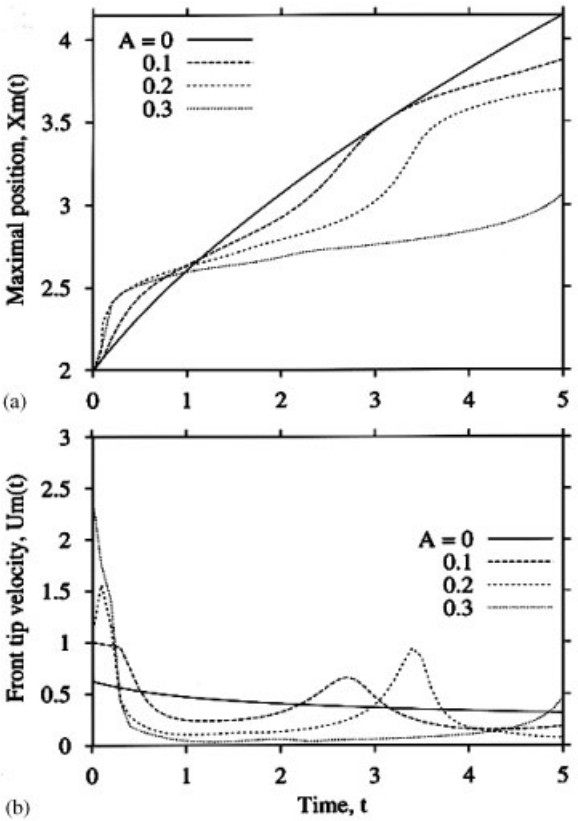

Figure 16. Influence of cavity modulation amplitude ($\omega = 6$): (a) evolution of the front tip position, X_m, with time; and (b) velocity at the front tip, $\mathrm{d}X_m/\mathrm{d}t$, with time.

The streamwise velocity distribution indicates that the most significant jump occurs at the walls ($y = 0$ and 2π), followed by a relatively important drop in U between the walls and the front tip ($y \approx \pi/2$ and $3\pi/2$), only to regain some strength at the tip ($y = \pi$). This is in sharp contrast with the flow in a non-modulated cavity, where the streamwise velocity at the front tip is the weakest. The corresponding spanwise velocity and phase plot indicate that the spanwise flow is essentially absent over the core region of the cavity ($2 < y < 4$). However, the spanwise flow gains considerable strength near the walls. The flow reaches the end of the contraction at $t = 1$. In this case, the flow diminishes considerably. The streamwise velocity, U, exhibits two maxima and a minimum at the tip. At $t = 2$, the fluid begins to move through the first cavity expansion, where it exhibits a behaviour similar to that in Figures 4–6. Some modulation is, however, present in the U and V distributions.

The overall influence of the modulation amplitude is depicted from Figures 16 and 17, for $\omega = 6$ and the range $A \in [0, 0.3]$. The case $A = 0$ corresponds to a cavity of constant thickness, and is included for reference. Figures 16(a) and 16(b) show the evolution of the front tip position, $X_m(t)$, and that of the tip velocity, $U_m(t)$. The figure shows that the sudden initial

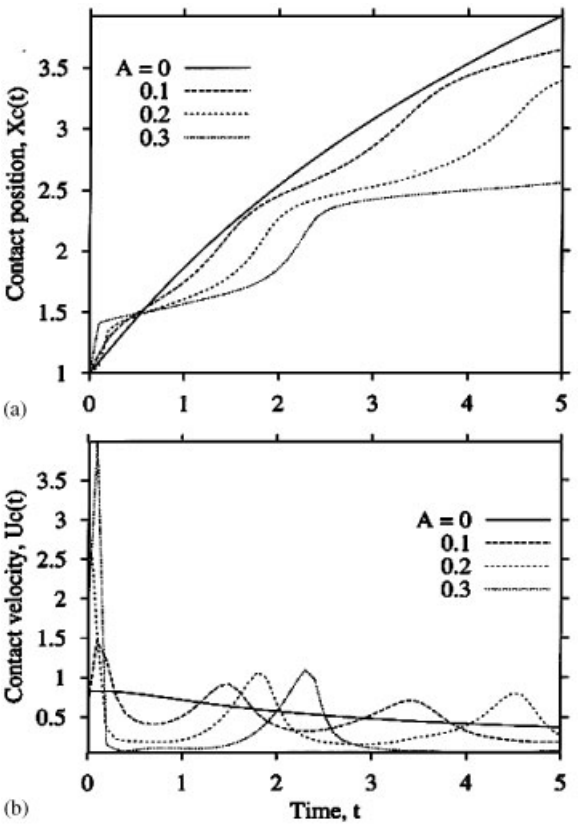

Figure 17. Influence of cavity modulation amplitude ($\omega = 6$): (a) evolution of the contact point position, X_c, with time; and (b) velocity at the contact point position, $\mathrm{d}X_c/\mathrm{d}t$, with time.

jumps in position and velocity increase with A. The jump is, however, followed by a sharp drop in U_m to an almost zero level. This corresponds to a leveling in X_m. There is a maximum in U_m that tends to occur at a later time as A increases. The trend is similar in Figure 17, where $X_c(t)$ and $U_c(t)$ are shown. However, the response at the contact with the walls is more modulated than at the front tip.

The effect of modulation frequency of the cavity walls is as significant as that of the amplitude. Figures 18 and 19 show the influence of $\omega \in [0, 6]$ for $A = 0.2$. Note that $\omega = 0$ corresponds to a flat cavity. For small ω, X_m begins to display some modulation, and U_m experiences a relatively weak maximum, which occurs later as ω increases. Another maximum appears initially as ω increases further. The emergence and timing of the maxima are more evident when U_c is examined (Figure 18(b)). These maxima tend to weaken as ω increases.

5. CONCLUSION

The general lubrication formulation is extended for transient free-surface flow inside thin three-dimensional symmetric cavities of thickness varying in the streamwise direction. The problem

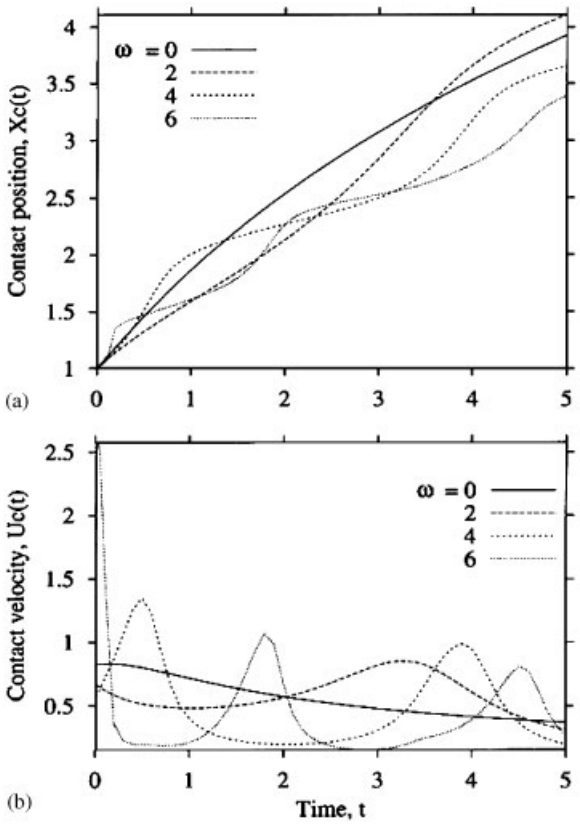

Figure 18. Influence of cavity modulation wavenumber ($A = 0.2$): (a) evolution of the front tip position, X_m, with time; and (b) velocity at the front tip, $\mathrm{d}X_m/\mathrm{d}t$, with time.

reduces to the Reynolds equation for pressure, coupled with front movement equation. A semi-analytical approach is used to solve the moving-boundary problem. The irregular and time-dependent domain is mapped onto the rectangular domain, and the transformed equations are solved by expanding the pressure and front position in Fourier series in the spanwise direction. The expansion coefficients are determined by solving the projected equations using an explicit forward difference scheme in time, and multiple-step finite-difference method in space. Three transient free-surface flow configurations are examined. In all cases, the driving pressure gradient is parabolic and maintained fixed at the cavity entrance. The initial domain occupied by the fluid is also parabolic. The flow inside a flat plate is studied first. In this case, the flow in the middle region tends to accelerate initially relative to the flow at the lateral walls. However, the slip at the walls eventually renders the front straight again, with considerable weakening of the spanwise flow. The flows inside contracting and expanding cavities are also examined. Although the evolution of the front is always monotonic with time, that of the velocity at the front can be oscillatory if the degree of contraction of the cavity is significant. The velocity of the contact point along the lateral walls is usually larger

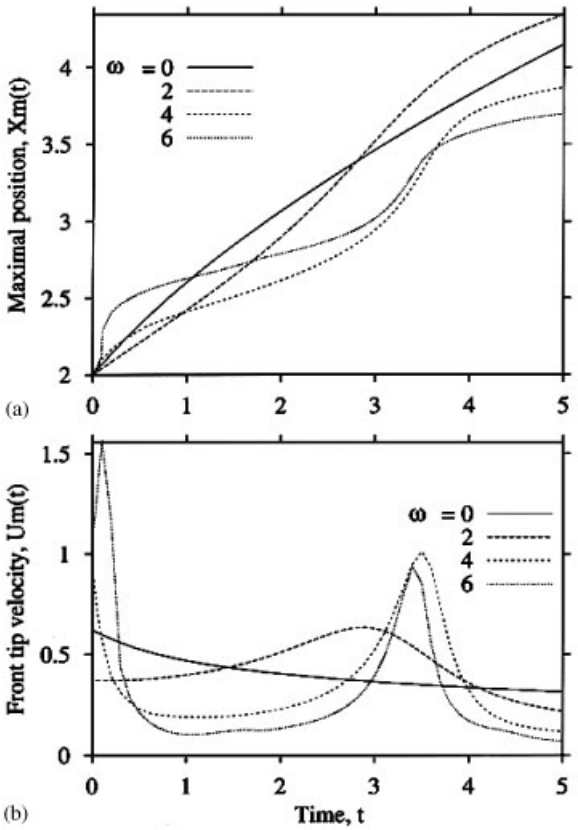

Figure 19. Influence of cavity modulation amplitude ($A = 0.2$): (a) evolution of the contact point position, X_c, with time; and (b) velocity at the contact point position, $\mathrm{d}X_c/\mathrm{d}t$, with time.

than that at the front. Finally, however, the flow inside a modulated cavity indicates that the slip velocity can be low enough to allow the front to advance at a faster rate, leading to its own undulation with a strong lateral flow. The fluid along the wall does not compress and expand simultaneously with the front centre (see Figure 14).

A number of assumptions were made in the present study that could easily relaxed if more complex flow configurations are contemplated. These assumptions are mainly of geometrical nature, namely related to cavity symmetry and thickness variation. For non-symmetric cavities, the formulation is generalized by taking a more general mapping than in Equation (13), and the pressure expansion (17) would have to include both cosine and sine terms. More general initial and conditions could easily accommodated including front shape and pressure variation and history. Although these issues are of importance, the major objective of the present work is to propose a methodology that is efficient and easy to implement to solve complex problems with a moving domain; only a few degrees of freedom are required for convergence. The complexity of the cases studied reflect the capabilities and potential of the proposed methodology.

ACKNOWLEDGEMENTS

The present work is supported by the Natural Sciences and Engineering Research Council of Canada.

REFERENCES

1. Hele-Shaw HS. The flow of water. *Nature* 1898; **58**:34.
2. Homsy GM. Viscous fingering in porous media. *Annual Review of Fluid Mechanics* 1987; **19**:271.
3. Park CW, Homsy GM. *Journal of Fluid Mechanics* 1984; **139**:291.
4. Hamrock BJ. *Fundamentals of Fluid Film Lubrication*. McGraw-Hill: New York, 1994.
5. Richardson S. Hele-Shaw flows with a free boundary produced by the injection of fluid into a narrow channel. *Journal of Fluid Mechanics* 1972; **56**:609.
6. Agassant JF, Avenas P, Sergent JPh, Carreau PJ. *Polymer Processing*: *Principles and Modeling*. Hanser Publishers: 1991.
7. Tadmor Z, Gogos CG. *Principles of Polymer Processing*. Wiley: New York, 1979.
8. Middleman S. *Fundamentals of Polymer Processing*. McGraw-Hill: New York, 1977.
9. Kamal MR, Kenig S. The injection moulding of thermoplastics. *Polymer Engineering and Science* 1972; **12**:294.
10. Winter HH. Approximate calculation and measurement of the pressure distribution in radial flow of molten polymers between parallel discs. *Polymer Engineering and Science* 1975; **15**:460.
11. Berger JL, Gogos CG. A numerical simulation of the cavity filling process with PVC in injection molding. *Polymer Engineering and Science* 1973; **13**:102.
12. White JL. Fluid mechanical analysis of injection mold filling. *Polymer Engineering and Science* 1975; **15**:44.
13. Broyer E, Gutfinger C, Tadmor Z. *Transactions of the Society of Rheology* 1975; **19**:423.
14. Van Wijngaarden H, Dijksman JF, Wesseling P. *Journal of Non-Newtonian Fluid Mechanics* 1982; **11**:175.
15. Williams G, Lord HA. Mold filling studies for the injection molding of thermoplastic materials. Part I. The flow of plastic materials in hot- and cold-walled circular channels. *Polymer Engineering and Science* 1975; **15**:553.
16. Alles H, Philipon S, Agassant JF, Vincent M, Debay G, Lerebours P. *Polymer Engineering and Science* 1986; **4**:71.
17. Agassant JF, Alles H, Philipon S, Vincent M. *Polymer Engineering and Science* 1988; **28**:477.
18. Hieber CA, Shen SF. A finite-element/finite-difference simulation of the injection molding filling process. *Journal of Non-Newtonian Fluid Mechanics* 1980; **7**:1.
19. Tucker CL, Folgar F. A model compression mold filling. *Polymer Engineering and Science* 1981; **23**:59.
20. Khayat RE, Derdouri A, Hebert LP. A boundary-element approach to three-dimensional gas-assisted injection molding. *Journal of Non-Newtonian Fluid Mechanics* 1995; **57**:253.
21. Khayat RE, Derdouri A, Frayce D. Boundary-element analysis of three-dimensional transient mixing processes of Newtonian and viscoelastic fluids. *International Journal for Numerical Methods in Fluids* 1998; **28**:815.
22. Shen SF. Simulation of polymer flows in the injection molding process. *International Journal for Numerical Methods in Fluids* 1984; **4**:171.
23. Barone MR, Oswald TA. Boundary element solution of filed problems. In *Computer Modeling for Polymer Processing. Fundamentals*, Tucker III CL (ed.). Hanser, 1989.

